

Direct Measurement of the Turbulent Kinetic Energy Viscous Dissipation Rate Behind a Grid and a Circular Cylinder

A. Ducci, E. Konstantinidis, S. Balabani and M. Yianneskis

Experimental and Computational Laboratory for the Analysis of Turbulence (ECLAT)
Department of Mechanical Engineering, King's College London
Strand, London WC2R 2LS, United Kingdom

Abstract

A method is presented to evaluate the turbulent kinetic energy viscous dissipation rate, ε , from the direct measurement of the mean squared turbulent velocity spatial gradients $\overline{(\partial u_i / \partial x_j)^2}$. The latter have been estimated using Laser Doppler Anemometer to measure simultaneously the velocities in two different points in the flow. To minimise the effect of virtual particle bias and of geometry bias the control volume dimensions have been reduced collecting the light in side scatter and using short focal length lenses. The methodology has been tested in the isotropic and homogeneous region of a turbulent flow downstream of a grid where ε is proportional to the kinetic energy decay. The measurements were carried out in a water rig for a Reynolds number Re_M of 5500, based on a mesh size M (5.5 mm) of the grid, along the centreline in a range between 23-35 M . Isotropic and homogenous conditions were satisfactorily achieved. In agreement with theory, the turbulent kinetic energy decayed exponentially along the centreline with a decay coefficient of 1.3. In Figure 1 the viscous dissipation rate derived from the kinetic energy decay (blue squares) is compared with the direct measurement ε (red circles) for different distances from the grid. The average difference between the two values along the centreline is about 7%. Further measurements were taken in the wake of a cylinder for a Reynolds number Re_d of 7200. The aim was to separate the contributions to the total kinetic energy viscous dissipation rate due to the periodic and the turbulent motions.

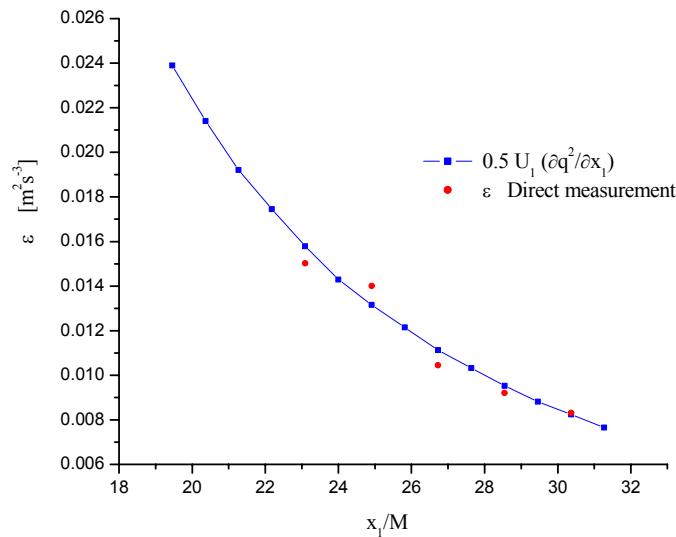


Figure 1 Decay of kinetic energy viscous dissipation rate along the centreline behind the grid using two different methods: dissipation derived from the kinetic energy decay (blue squares); direct measurement of ε (red circles)

1. Introduction

The knowledge of the rate of dissipation of turbulence kinetic energy per unit mass, ε , is of great importance in fluid mechanics, e.g. many turbulence models include an equation for ε and therefore is essential for testing the applicability of the models commonly used. However its accurate experimental determination poses a challenging problem. The rate of dissipation of turbulence kinetic energy is defined as follows Hinze (1975):

$$\varepsilon = \nu \overline{\left(\frac{\partial u_i}{\partial x_j} + \frac{\partial u_j}{\partial x_i} \right) \frac{\partial u_j}{\partial x_i}} \quad (1)$$

These limitations are usually overcome assuming, even for more complex flows, local isotropy, simplifying equation (1) as follows:

$$\varepsilon = 15 \nu \overline{\left(\frac{\partial u_1}{\partial x_1} \right)^2} \quad (2)$$

As pointed out by Elsner & Elsner (1996), with this hypothesis the different terms comprising the dissipation equation are related as follows:

$$K_{jj} = \frac{\overline{\left(\frac{\partial u_j}{\partial x_j} \right)^2}}{\overline{\left(\frac{\partial u_1}{\partial x_1} \right)^2}} = 1 \quad (3)$$

$$K_{ijij} = \frac{\overline{\left(\frac{\partial u_i}{\partial x_j} \right)^2}}{\overline{\left(\frac{\partial u_1}{\partial x_1} \right)^2}} = 2 \quad \text{for } i \neq j \quad (4)$$

$$K_{ijji} = \frac{\overline{\left(\frac{\partial u_i}{\partial x_j} \right) \left(\frac{\partial u_j}{\partial x_i} \right)}}{\overline{\left(\frac{\partial u_1}{\partial x_1} \right)^2}} = -\frac{1}{2} \quad \text{for } i \neq j \quad (5)$$

The assumption of homogeneous turbulence is less restrictive than that of isotropic turbulence and assuming symmetric flow ($u_2 = u_3$) and symmetric geometry ($\partial/\partial x_2 = \partial/\partial x_3$), equation (1) becomes:

$$\varepsilon = \nu \left[\overline{\left(\frac{\partial u_1}{\partial x_1} \right)^2} + 2 \overline{\left(\frac{\partial u_3}{\partial x_3} \right)^2} + 2 \overline{\left(\frac{\partial u_1}{\partial x_3} \right)^2} + 2 \overline{\left(\frac{\partial u_3}{\partial x_1} \right)^2} + 2 \overline{\left(\frac{\partial u_3}{\partial x_2} \right)^2} \right] \quad (6)$$

In the published literature, (e.g. Tennekes & Lumley (1973)), nearly homogeneous and isotropic flow is usually assumed to be reached behind a grid, where the wakes created by the rods merge together, after an initial region of high inhomogeneity and anisotropy. As described by Tennekes & Lumley (1973), in the homogeneous and isotropic region the equation for the turbulence mean kinetic energy can be simplified as follows:

$$\frac{\overline{U}_1}{2} \left(\frac{\partial \overline{q^2}}{\partial x_1} \right) = -\varepsilon \quad (7)$$

The rate of change of the kinetic energy in time (the convective term) is equal to the viscous dissipation, so that $\overline{q^2}$ decays constantly along the axis X_1 of the main flow, following a relationship of the form:

$$\frac{\overline{u^2}}{\overline{U}_1^2} = A \left(\frac{x}{M} - \frac{x_0}{M} \right)^{-n} \quad (8)$$

where M is the mesh spacing, n is the exponent characterising the decay of turbulence, x is the distance from the grid, and x_0 is a virtual origin which accounts for the fact that the effective origin of the velocity fluctuations may not coincide with the location of the grid.

In the earliest study of grid generated turbulence, referred to in Comte-Bellot & Corssin (1966), the values of n and x_0/M varied respectively from 1 - 1.3 and 0 - 10, depending on the initial conditions such as mesh size M , rod shape (parallelepipedal or cylindrical), solidity ratio σ , and mesh Reynolds number Re_M .

There have been many studies of grid turbulence since this seminal work of Comte-Bellot & Corssin (1966). The description of the flow has, in general, improved with the accuracy of the measurement techniques and for this reason only the most recent relevant works are considered below.

Mohamed & LaRue (1990) performed an extensive study of this flow in a wind tunnel and reviewed some of the earliest works. They emphasised that using only data belonging to the homogeneous isotropic region, n and x_0/M do not depend on the initial conditions and assume values around 1.30 and 0 respectively. They suggested different methods to determine the beginning of the isotropic region: the skewness of the velocity fluctuation $S(u)$ and of the velocity derivative $S(du/dx)$ should be equal to 0 and to a constant respectively, and the ratio between the dissipation calculated with equation (7), for grid turbulence flow, and with the equation (2), for local isotropic flow, should be 1 for the entire homogeneous and isotropic region. As Re_M was decreased, the start of the homogeneous area was found to be located closer to the grid.

In addition to the method used by Mohamed & LaRue (1990), Tresso & Munoz (2000) determined also the beginning of the isotropic and homogenous region for different initial conditions, by applying directly the definition of isotropy ($u_1 u_2 = 0$). Using this approach they determined an experimental law describing the beginning of the isotropic and homogeneous region as a function of Re_M .

In agreement with Mohamed & LaRue (1990), Zhou *et al.* (2000), measuring at a distance x/M higher than 20, obtained an exponent n equal to 1.33 and a value of x_0 equal to 0.

The flow conditions and the main results of the aforementioned works are summarised in Table 1:

Table 1. *The decay power-law exponent (n), coefficient (A) and other parameters in previously published works.*

Ref.	$Re_M \times 10^{-3}$	Fluid	Beginning of Isotropic Hom. Region	n	A	x_0/M	σ	M/d
Comte-Bellot & Corssin (1966)	135-17	Air	20*	1.1-1.33	0.05	3-5	0.31-0.44	-
Mohamed & LaRue (1990)	6	"	25	1.30	0.0435	0	0.34	5.4
	10	"	40	1.30	0.0424	0	"	5.4
	14	"	50	1.28	0.0364	0	"	5.4
	12	"	55	1.29	0.0490	0	"	5.3
Zhou <i>et al</i> (2000)	10.5	"	30*	1.33	-	0	0.35	5.2
Tresso & Munoz [2000]	10.7	"	18	-	-	-	0.28	8
	22.9		28					
	34		57					
* These works did not evaluate the coordinate x/M where the flow becomes isotropic and homogeneous. This value identifies the distance from the grid where the first measurements were made. (-) This symbol means that the parameter is not available								

Direct measurement of the spatial gradients using a two channel LDA was attempted by Michelet (1998) in grid turbulence flow. Because of the difficulty encountered in measuring the decay of the kinetic energy ($n=0.33$), Michelet (1998) compared the values of the dissipation using equation (6) for homogeneous flow and equation (2) for local isotropic turbulence. The latter was computed by integrating the energy spectrum of the velocity fluctuations. The agreement obtained was excellent, but the expressions of the equations applied leave some doubt as to the validity of the results.

Another work which attempted to calculate directly the spatial gradients, has been reported by Benedict & Gould (1996). The intention of that work was to calculate the gradients by estimating the Taylor micro scale from the spatial correlation coefficients $R_{ii}(\Delta x_j)$ and $R_{ij}(\Delta x_i)$ in sudden contraction flow. They pointed out how the dimensions of the control volumes affect the accuracy of the determination of the spatial correlation coefficient, as a control volume which is too large gives a poor resolution of $R_{ii}(\Delta x_j)$. They suggested that for a proper estimation of $R_{ij}(\Delta x_j)$ the control volume should be of the order of the Kolgomorov scale.

Apart from the necessity to have an isotropic and homogeneous flow, it is necessary to discuss the errors involved in multidimensional LDA measurement. Three types of bias are relevant in such systems.

Boutier *et al* (1985) considered the possibility that in 3-D LDA measurements two different particles could satisfy a simultaneity criterion, crossing the control volumes within a defined time interval, even if they would not pass through the overlapping region. This results in a source of error, termed virtual particle bias, which leads to a substantial underestimation of the Reynolds stresses.

The second type of bias, the geometry bias, was firstly determined by Brown (1989); he established that even a single particle, with a consistent velocity component in the plane containing the axis of the two control volumes, could pass outside the overlapping region within the time coincidence window.

The effect of the third type of bias, the time coincidence bias, was determined by Benedict & Gould (1996) during their study of the spatial correlation coefficient. When the two control volumes are separated by a small distance along the direction of the dominant velocity of the flow, it is possible that a single particle will cross both the control volumes within the time coincidence window, resulting in an overestimation of the correlation coefficient.

2. Flow configuration, LDA system and measurement procedure

The rig consists of a single loop pipe arrangement with a by-pass and a centrifugal pump, which directs the water into an expansion/contraction section containing a hexagonal honeycomb to straighten the flow. A perforated plate is placed downstream the contraction to reduce the turbulence levels before the flow reaches the grid. The measurements are taken in the second half of a transparent acrylic test section to allow the flow to become homogeneous and isotropic. A heat exchanger jacket in a tank downstream of the test section maintains the temperature of the water at a constant value. The dimensions of the grid and of the test section used are shown in following Table 2:

Table 2. Test section and grid dimensions

Test section dimensions (W x W x L)	Grid	
	Mesh size (M)	Wire diameter (D)
72 x 72 x 184 mm ³	5.5 mm	1 mm

The LDA employed is a Dantec system and comprises three probes mounted on a transverse that can be remotely moved in all the directions. One of the probes can measure two velocity components while the others can measure only one. The probes are designed to work in the back-scatter mode.

The arrangements of the probes for the measurements of the gradients $(\partial u_1 / \partial x_1)^2$, $(\partial u_1 / \partial x_3)^2$, $(\partial u_3 / \partial x_3)^2$, $(\partial u_3 / \partial x_1)^2$ are shown in Figure 2. The two-channel probe shown in blue is displaced along the directions indicated. Depending on the gradient of interest, the green probe measures the u_1 velocity (Figure 2.(a)) or the u_3 velocity (Figure 2.(b)). The blue and green probes incorporate lenses of focal length 240 mm and of 310 mm respectively. The control volume dimensions for the lenses mounted on the three probes are shown in Table 3.

To reduce the longer dimension of the green control volume the light scattered by the 10 μm diameter particles is collected in side scatter by the red probe. The red probe incorporated a lens of focal lens 310 mm or 500 mm depending on the arrangement (Figure 2 (a) or (b) respectively) to ensure that all three lenses focused at the same point.

Accurate calculation of the effective size of the control volume in side scatter is not possible because, even if the diameter of the fibre optic cable (50 μm), substituting in this system the pinhole usually placed in front of the photomultiplier, is known, the exact lens magnifying power is unknown. From geometry considerations, taking in to account that the angle between the optical axes of the side probes and of the centre probe is about 22°, the longer dimension of the green control volume for side scatter should be around 0.24 mm.

Table 3. Focal length and control volume dimensions, in back scatter, of the lenses employed

Probe	Focal length	Diameter dx1	Diameter dx2	Length dx3
Blue Probe	240 mm	0.05 mm	0.05 mm	0.37 mm
Green probe	310 mm	0.07 mm	0.07 mm	0.63 mm
Red Probe	310 mm	0.07 mm	0.07 mm	0.63 mm
	500 mm	0.125 mm	0.124 mm	1.7 mm

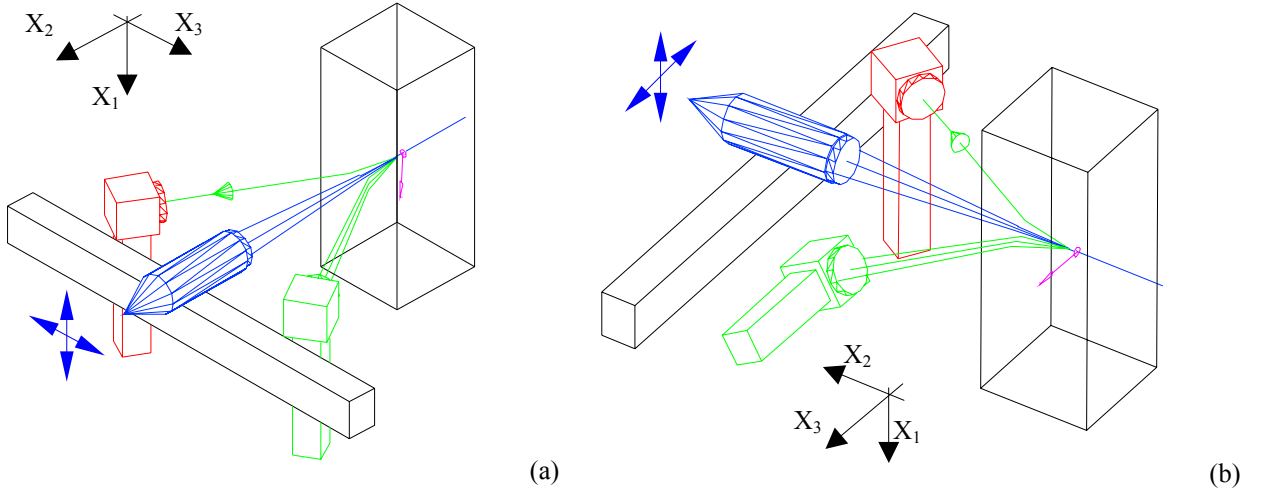


Figure 2 Probe arrangement to measure the velocity gradients: (a) $\overline{(\partial u_1 / \partial x_1)^2}$, $\overline{(\partial u_1 / \partial x_3)^2}$; (b) $\overline{(\partial u_3 / \partial x_3)^2}$, $\overline{(\partial u_3 / \partial x_1)^2}$.

The probes are aligned in air using a pinhole of 50 μm . Once in water, to overcome the effect of refraction, it is necessary to adjust the relative position of the three control volumes along the X_2 axis by a known distance. As suggested by Benedict & Gould (1996) a further optimisation of the alignment is achieved computing the spatial correlation coefficient $R_{ii}(0)$ for different relative positions of the probes until a maximum is found.

The spatial gradients $\overline{(\partial u_i / \partial x_j)^2}$ are estimated calculating the function $f_{ii}(\Delta x_j)$ defined in (9) for the different positions examined around the reference point x_i :

$$f_{ii}(\Delta x_j) = \overline{(u_i(x_j, t) - u_i(x_j + \Delta x_j, t))^2} \quad (9)$$

When computing the coefficient $f_{ij}(\Delta x_j)$, the velocity fluctuations u_i in the two different points of measurement must come from particles which cross the two control volumes at the same time. This condition is imposed by finding the couples of particles that satisfy the following simultaneity criterion:

$$|t_1 - t_2| < \tau_w, \quad (10)$$

where t_1 and t_2 are the arrival time and τ_w is a time coincidence window.

Once the function $f_{ij}(\Delta x_j)$ is known, the spatial gradient can be calculated from (11)

$$\overline{\left(\frac{\partial u_i}{\partial x_j}\right)^2} = \lim_{\Delta x_j \rightarrow 0} \frac{\overline{(u_i(x_j, t) - u_i(x_j + \Delta x_j, t))^2}}{\Delta x_j^2} \quad (11)$$

The spatial gradient can be evaluated by finding the slope of the straight line which best fits the points $(\Delta x_j^2, f_{ii}(\Delta x_j))$ for Δx_j values close to zero. Once all the gradients have been determined, the value obtained for the dissipation rate estimated from equation (6) for homogenous flow is compared with the value obtained from equation (7) for grid turbulence flow.

3. Grid turbulence flow

The experiments were carried out along the centreline of the test section for a mesh Reynolds number Re_M of 5500. Figure 3 shows the rate of decay of the kinetic energy and of the turbulence intensities $\overline{u_1^2}/\overline{U_1^2}$ and $\overline{u_3^2}/\overline{U_1^2}$ along the X_1 direction. It is evident that the flow is not perfectly isotropic as the turbulence intensities along axis X_1 and X_3 are not the same. This difference was also present in previous works, such as Comte-Bellot & Corssin (1966) and Zhou et al. (2000) and wasn't considered to be significant, as the difference between the rms values in the two directions is within the accuracy of the LDA system.

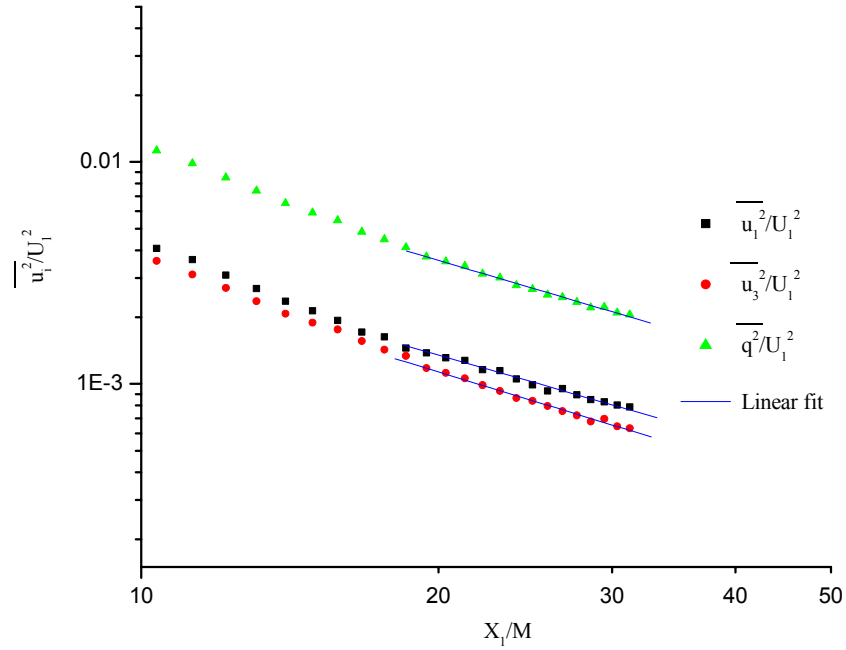


Figure 3 Decay of $\overline{q^2}/\overline{U_1^2}$, $\overline{u_1^2}/\overline{U_1^2}$ and $\overline{u_3^2}/\overline{U_1^2}$ along the duct centre line

As suggested by Mohamed and Larue (1990), the coefficients of the exponential law shown in (8) have been estimated applying a least-squares linear regression between points belonging to the homogenous and isotropic region. This is found to begin at a distance of 20 M from the grid. Considering that Mohamed & Larue (1990) determined that the beginning of the isotropic and homogeneous region is closer to the grid as Re_M is decreased, this value should be considered in good agreement with the others shown in Table 1. The decaying coefficients n found for $\overline{q^2}/\overline{U_1^2}$, $\overline{u_1^2}/\overline{U_1^2}$ and $\overline{u_3^2}/\overline{U_1^2}$ are 1.31, 1.27 and 1.35 respectively.

4. Rate of dissipation for the grid turbulence flow

The direct measurement of the spatial gradients has been carried out between 20 and 35 M for a Re_M of 5500. In Figure 4 the values assumed by $f_{ii}(\Delta x_j)$ at a distance of 23 M from grid, are plotted against Δx_j^2 for all the gradients measured. The time coincidence windows τ_w applied is of 0.03 ms. All the $f_{ii}(\Delta x_j)$ have been evaluated for distances Δx_j between 0-0.7 mm with a step of 0.1 mm.

Considering Figure 4, it can be observed that the values of $f_{ii}(\Delta x_j)$ for $\Delta x_j^2 > 0$ are much higher than for $f_{ii}(0)$. This substantial difference has to be attributed to the relatively large dimensions of the control volume. On the one hand, when the probes are displaced, it is very unlikely that two particles will cross the centre of the two control volumes at the same time to give a highly correlated pair of velocity values. It is more probable that one of them will pass through the centre of one control volume while the other will pass far away from the centre of the second control volume, resulting in a higher distance between the points where the control volumes are crossed than the effective displacement Δx_j effectuated. This leads to velocity pairs less correlated than expected. On the other hand, when

the two probes are aligned at the same point, each particle crossing one control volume will more likely cross the second control volume in the same point giving always highly correlated velocity pairs.

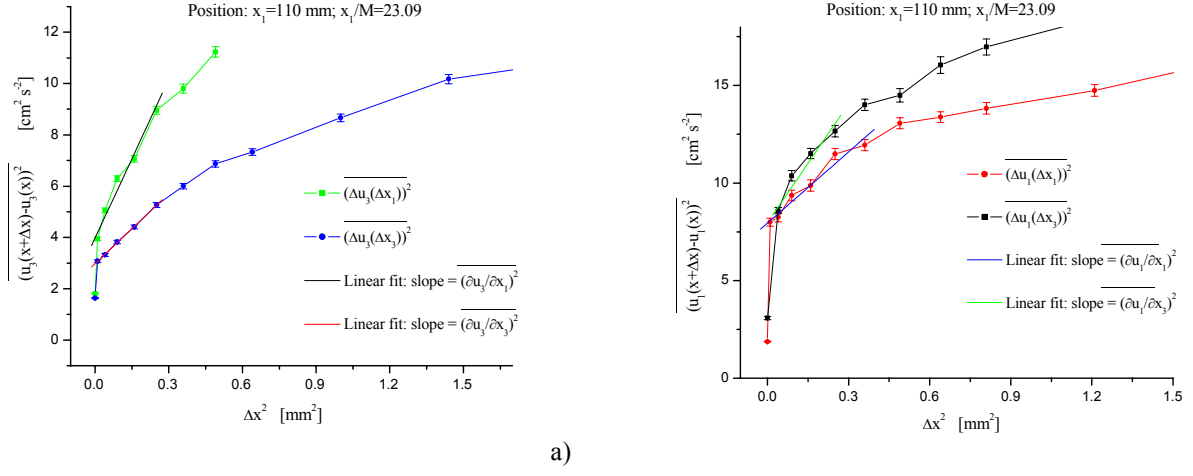


Figure 4 Variation of $f_{ii}(\Delta x_j)$ with Δx_j^2 in $x_1/M=23.09$: (a) $(\partial u_3/\partial x_3)^2$, $(\partial u_3/\partial x_1)^2$; (b) $(\partial u_1/\partial x_1)^2$, $(\partial u_1/\partial x_3)^2$.

The same effect is evident also in Figure 5 where the variation of the spatial correlation factors $R_{33}(\Delta x_3)$ and $R_{33}(\Delta x_1)$ is plotted against Δx_j . The value of $R_{33}(\Delta x_j)$ for Δx_j equal to zero is much higher than those for Δx_j different than zero. For this reason the $(0, f_{ii}(0))$ pairs have not been considered in the line fitting to determine the spatial gradient values.

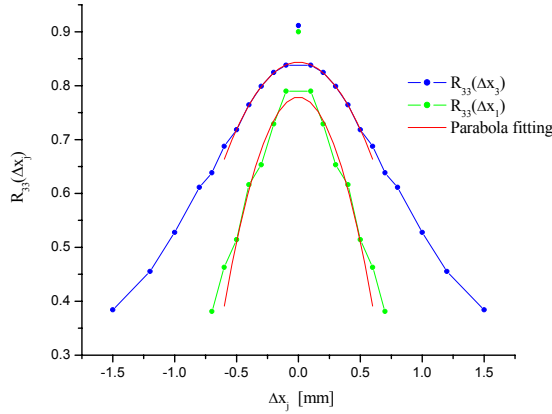


Figure 5 Correlation factors $R_{33}(\Delta x_3)$ and $R_{33}(\Delta x_1)$ in x_1/M of 23.09

As can be seen in Figure 4 the value of $R_{33}(0)$ is 0.92 and far from the ideal correlation coefficient that should be 1 for Δx_j equal to zero. There are three main reasons to explain this difference. The first one has to be attributed to the size of the control volume which, despite the small dimension, is still too big for a perfect correlation. The second one is due to the noise level. In fact the necessity to have a sufficient amount of data in coincidence between the two channels leads to use higher values of the High Voltage (HV). This was confirmed through trials with a decreasing HV, for which the correlation reached a maximum value of 0.96. The third, probably the most important, has to be attributed to the flow and the limits of the BSA. In fact the turbulence level is very small so that the correlation and the f_{ii} value depends mostly on the second decimal digit of the velocity fluctuation value. This problem is more visible if the light scattered by the same control volume is collected from two different probes, one in back scatter and one in side

scatter. Despite the velocities measured belonging for certain to the same particles, the correlation value is 0.96. Therefore this value has to be considered as the intrinsic error of the system.

The perfect symmetry of the two correlation functions represent in Figure 4 is artificial and not experimental. To plot the parabola best fitting the points illustrated in Figure 4, $R_{33}(-\Delta x_j)$ has been set equal to $R_{33}(\Delta x_j)$. Considering in Figure 4 the fitted lines for the four different spatial gradients, it is possible to appreciate qualitatively how the slopes of the gradients $(\partial u_1/\partial x_3)^2$ and $(\partial u_3/\partial x_1)^2$ are higher and around twice the slopes of $(\partial u_1/\partial x_1)^2$ and of $(\partial u_3/\partial x_3)^2$ respectively. This is visible also in Figure 5 where the parabola fitted between the $R_{33}(\Delta x_1)$ values is narrower than that fitted in $R_{33}(\Delta x_3)$. The variation of the spatial gradients

$\overline{(\partial u_1/\partial x_1)^2}, \overline{(\partial u_3/\partial x_1)^2}, \overline{(\partial u_1/\partial x_3)^2}, \overline{(\partial u_3/\partial x_3)^2}$ along the duct centreline is plotted in Figure 6. The gradients have been evaluated by fitting a line between the values of $f_{ii}(\Delta x_j)$ for Δx_j varying between 0.1-0.6 mm. This corresponds to a range of 1-5 Kolgomorov scale η . The best fitting line has been found maximising the correlation factor R of the linear interpolation. Regardless of the experimental scatter of the gradient values, the isotropic conditions illustrated in equations (3), (4) are satisfactorily achieved.

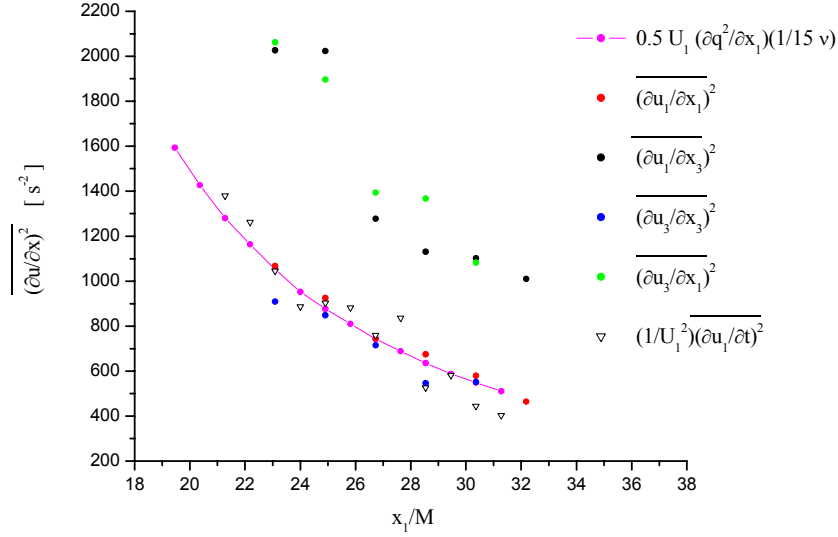


Figure 6 Comparison between the values assumed by the spatial gradients directly measured (red, black, blue and green circles) and the $\overline{(\partial u_1/\partial x_1)^2}$ gradient calculated from the kinetic energy decay (violet line) and from Taylor's hypothesis (triangles).

In Figure 6 the values of the spatial gradients measured directly are compared with the values of $\overline{(\partial u_1/\partial x_1)^2}$ calculated with the kinetic energy decay and with Taylor hypothesis. The latter gradients have been calculated applying the slotting technique (Van Maanen & Tummers (1996)), normally used to determine the autocorrelation coefficient. In the present work the technique is used to evaluate the f_{ii} coefficients for different time intervals Δt . Even in this case the time coincidence window used is 0.03 ms. The different methods implemented show a good agreement.

A comparison between the values of the scaled dissipation ($\varepsilon M/\overline{U_1^3}$) from the present and previous works is shown in Figure 7. The dissipation values are calculated from the kinetic energy decay. The coefficients A and n of the kinetic energy decay have been taken from Mohamed & LaRue (1990) who, as already mentioned, revisited some of the earliest work on grid turbulence flow. The non dimensional dissipation values have been plotted for X_1/M in the range of 20-40 M. The values of $\varepsilon M/\overline{U_1^3}$ shown in Figure 7 differ by a large amount (46 % difference between the values of the curves located furthest away from each other).

Considering the high values of Re_M used in some of the past works, it is possible that for some of them the isotropic region commenced somewhere in the range or even at higher distances from the grid, but this do not affect the validity of the graph. In fact the dissipation decaying coefficients (1+n) of the curves plotted vary by small amounts (2.26-2.35), so that can be assumed that all the curves remain parallel to each other and their differences do not become smaller for higher values of x_1/M . The high difference between the scaled values $\varepsilon M/\overline{U_1^3}$ is due to the substantial variation of A (0.0364-0.0664) from one work to the other. From Figure 7 it can be observed that the values of $\varepsilon M/\overline{U_1^3}$ of the present work lie between the curves of the previous works.

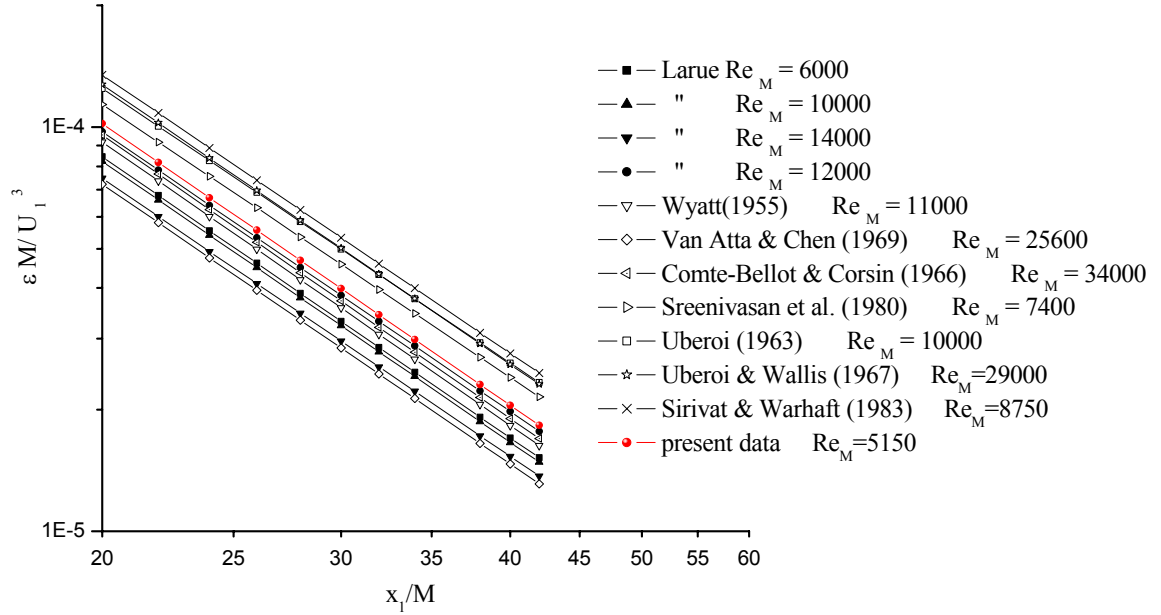


Figure 7 Comparison between the values assumed by the dimensionless dissipation $\varepsilon M / \overline{U}_1^3$ in the present and in previous works.

The comparison between the values of the dissipation calculated from the decay of kinetic energy and from the direct estimation of the gradients have been illustrated in Figure 1. According to the isotropic relation (4), the contribution to dissipation due to the spatial gradient $(\overline{\partial u_3 / \partial x_2})^2$ in (6) have been substituted with the spatial gradients $(\overline{\partial u_1 / \partial x_3})^2$ and $(\overline{\partial u_3 / \partial x_1})^2$.

5. Flow in the wake of a cylinder

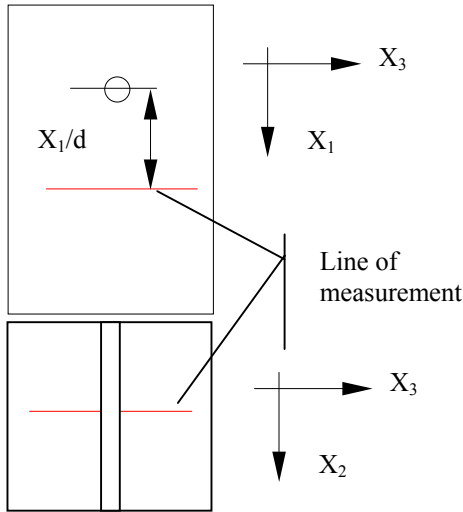


Figure 8 Diagram showing the locations where the measurements were taken

The measurements were carried out across the wake of the cylinder along a line parallel to the X_3 direction located in the centre of the test section and at a distance from the cylinder of X_1/d equal to 10 (Figure 8). The points of measurements are X_3/d : -0.2, -0.1, 0, 0.1, 0.2, 0.3, 0.4, 0.5, 0.8, 1.2, 1.6, 2. The Reynolds number Re_d is 7200 and the diameter d of the cylinder is 7.2 mm.

The method used to determine the gradients is the same as described earlier for the grid turbulence flow. In this case it is necessary to separate the turbulence from the periodic motions due to the presence of mean flow variations due to vortex shedding. As for the grid turbulence flow, the two data series, one from each of the two probes, have been scanned to find the particles that satisfy the condition of equation (10).

The periodic motions have been identified by low pass filtering the spectra of the two data series.

In Figure 9 the total velocities of the particles in coincidence and the velocities due to the periodicity of the flow (the low pass filtered velocities) are shown.

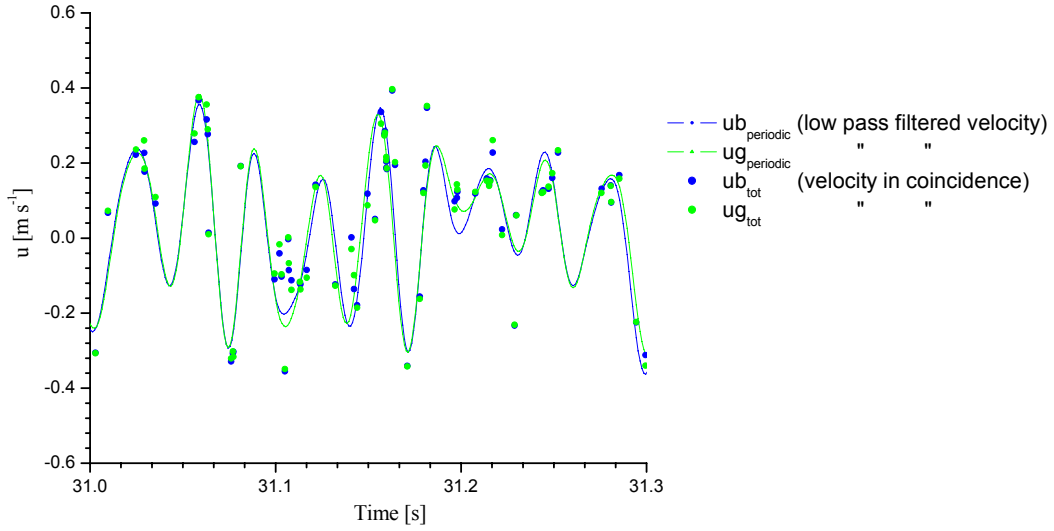


Figure 9 Comparison between the values of the low pass filtered velocity and the total velocity of the particles in coincidence for each channel (blue and green).

Considering that the frequency of the periodical motion is 30 Hz, the data have been low pass filtered up to a frequency of 50 Hz. The turbulent velocities have been calculated by subtracting the periodic velocity from the total velocity of the particles in coincidence. The variations of the spatial gradients values against X_3/d are shown in Figure 10. The gradients have been calculated by determining the slopes of the lines providing the best fit of the pairs $(\Delta x_j, f_{ii}(\Delta x_j))$ for Δx_j varying between 0.1-0.3 mm.

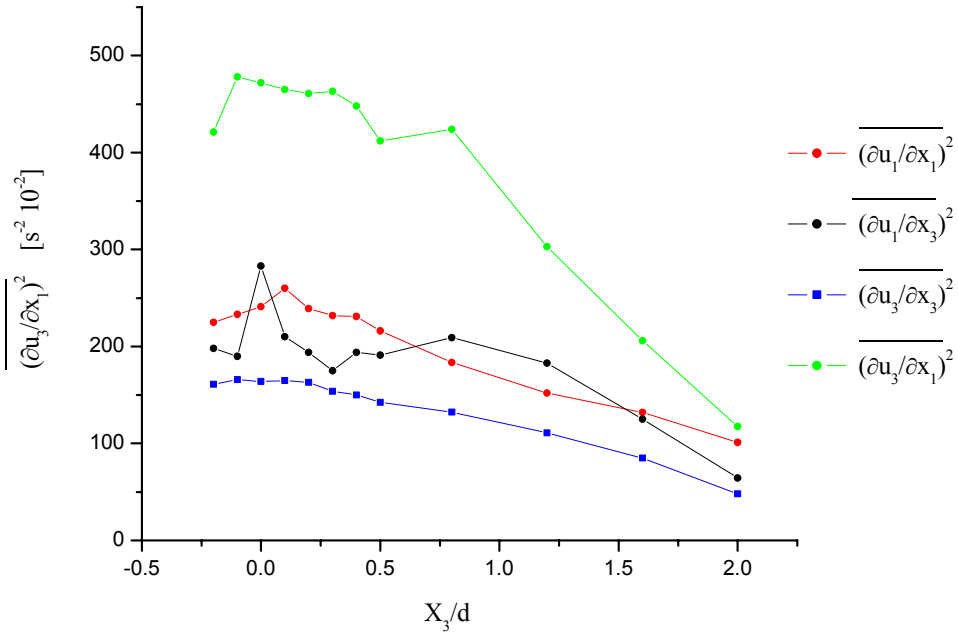


Figure 10 Variations of the spatial gradients $\overline{(\partial u_3/\partial x_3)^2}$, $\overline{(\partial u_3/\partial x_1)^2}$, $\overline{(\partial u_1/\partial x_1)^2}$, $\overline{(\partial u_1/\partial x_3)^2}$ values with X_3/d .

6. Conclusions

A LDA method to measure the spatial gradients contributing to the kinetic energy viscous dissipation rate has been presented.

In the first part of the paper the method has been tested to determine the gradients in grid turbulence flow. The gradients have been estimated finding the line best fitting the pairs $(\Delta x_j, f_{ii}(\Delta x_j))$ with $\Delta x_j/\eta$ varying between 1-5. The isotropic conditions shown in (3) and (4) have been satisfactorily achieved. Moreover the values of dissipation calculated adding the contributions of the different gradients are comparable with the values of dissipation derived from the kinetic energy decay for homogeneous flow.

In the second part of the paper the method was applied to a cylinder flow. The results show that in both cases ε can be determined with good accuracy with the present LDA system.

These studies in fact have been conducted partly in order to establish the suitability of the ε measurement technique in a relatively simple flow, before its application to measure the dissipation rate in a stirred vessel.

Roman characters

Symbols		Units
A	Coefficient in the turbulence decay law for grid generated turbulence, equation	-
d	Cylinder diameter	m
D	Grid wire diameter	m
dx_i	Control volume dimension in the X_i direction	m
$f_{ii}(\Delta x_j)$	Mean of the squared difference of the values of the i-th velocity fluctuation component measured at a distance Δx along the j-th direction	-
L	Test section length	m
M	Grid wire mesh spacing	m
n	Decay exponent of kinetic energy in grid generated turbulence	-
$\overline{q^2}$	Mean turbulence kinetic energy	$m^2 s^{-2}$
Re_d	Cylinder flow Reynolds number based on the diameter	-
Re_M	Mesh Reynolds number	-
$R_{ii}(\Delta x_k)$	Space correlation coefficient between the values of the i-th velocity fluctuation component at a distance Δx along the k-th direction	-
t_i	Arrival time of a particle in the control volume	s
U_i	Velocity component along the i-th direction	$m s^{-1}$
u_i	Velocity fluctuation along the i-th axis	$m s^{-1}$
$\overline{U_i}$	Mean velocity along the i-th axis	$m s^{-1}$
W	Test section side	m
x_0	Virtual origin value of the velocity fluctuations in grid generated turbulence along the axis of the test section	m

Greek characters

Symbols		Units
Δt	Time interval	s
Δx_i	Displacement along the i-th axis	m
$\overline{(\partial u_i / \partial x_j)^2}$	Spatial gradient of u_i velocity fluctuation along j-th axis	s^{-2}
ε	Kinetic energy viscous dissipation rate	$m^2 s^{-3}$
ν	Kinematic viscosity	$m^2 s^{-1}$
σ	Solidity ratio	-
τ_w	Time coincidence window	s

Abbreviations

BSA	Burst spectrum analyser
LDA	Laser Doppler anemometer

References

- Benedict, L. H. and Gould, R. D. (1996). "Understanding biases in the near field region of LDA two-point correlation measurements", Proc. 8th Int. Symposium on Applies of Laser Techniques to Fluid Mechanics, Lisbon, paper 36.6..
- Boutier, A., Pagan, D. and Soulevant, D. (1985). "Measurement Accuracy with LDV Laser Velocimetry", Tp 171, ONERA.
- Brown, J. L. (1989). "Geometric Bias and Time coincidence in 3-dimensional Laser Doppler Velocimeter systems", Exp. Fluids, 7:25-32.
- Comte-Bellot, G. and Corrsin, S. (1966). "The use of contraction to improve the isotropy of grid generated turbulence", J Fluid Mech., 25, part 4: 657-682.
- Elsner, J. W. and Elsner, W. (1996). "On the measurement of turbulence energy dissipation", Meas. Sci. Technol. 7:1334-1348.
- Hinze, J.O. (1975). "Turbulence", McGraw-Hill, 2nd edition.
- Michelet, S. (1998). "Turbulence et dissipation au sein d'un reacteur agite par une turbine Rushton-velocimetrie laser Doppler a deux volumes de mesure", Phd Thesis, L'Institut National Polytechnique de Lorraine.
- Mohamed, M. S. and Larue, J. C. (1990). "The decay power law in grid generated Turbulence", J. Fluid Mech., 219: 195-214.
- Tennekes, H. and Lumley, J.L. (1973). "A first course in turbulence", The MIT Press.
- Tresso, R. and Munoz, D. R. (2000). "Homogeneous, Isotropic Flow in Grid Generated Turbulence", Journal of Fluid Engineering., 122: 51-56.
- Van Maanen, H.R.E. and Tummers, M., (1996). "Estimation of the Auto Correlation Function of Turbulent Velocity Fluctuation using the Slotting Technique with Local Normalisation"., Proc. Symposium on Applies of Laser Techniques to Fluid Mechanics, Lisbon, paper 36.4..
- Zhou, T., Antonia, R. A., Danaila, L. and Anselmet, F. (2000). "Transport equations of the mean energy and temperature dissipation rates in grid turbulence", Exp. Fluids, 28:143-151.

